Nucleon and light nucleus emission from excited nuclei

C. Bonilla, G. Royer, F. Sébille, V. de la Mota
Laboratoire Subatech, 4 rue A. Kastler, 44072 Nantes Cedex 03, France
(celine.bonilla@subatech.in2p3.fr)

Abstract : The emission of clusters by excited nuclei is adressed within two approaches. The DYWAN model describes the dynamics of nucleon nucleus collisions thanks to a strongly compressed representation of the nuclear system with a wavelet basis. This approach leads to predictions for nucleon and cluster emission, while allowing to explore the characteristics of reaction mechanisms, such as the sensitivity to mean-field and in-medium effects. In a second approach, we used a Generalized Liquid Drop Model to investigate a particular decay channel: light nucleus emission for excitation energy below the barrier. The half-lives have been determined within a tunneling process through the potential barrier given by this model. Analytical formulae allowing to obtain rapidly these different partial half-lives are proposed.

1 Introduction

The conception and development of Accelerator Driven System for the transmutation of nuclear waste and the production of energy requires the study of spallation reactions, that is to say, the interaction between a nucleon beam and a target, often lead or lead-bismuth, which induces the formation of an excited system giving rise to the emission of nucleons and clusters. In this work, these reactions are described in two different ways. The first one proposes a description of the dynamics of the reaction based upon the ETDHF equation solved thanks to the projection of the single-particle wavefunctions on a wavelet basis. In this work, some results of the simulation for the nucleon and clusters emission are given, and some physical aspects of these reactions are investigated. In the second approach, a specific decay channel is presented: the light nucleus emission from a mother nucleus having an excitation energy lower than the decay barrier height. More precisely the Be, Li, He and H decay half-lives of slightly excited nuclei have been determined within a tunneling process through a potential barrier calculated from a Generalized Liquid Drop Model with quasimolecular shapes.

2 Description of the nucleon-nucleus collisions with the DYWAN model

2.1 Bases of the model

The mechanism of nucleon-nucleus collisions strongly depends on the energy of the incident nucleon. Below 20 MeV there are mostly pre-equilibrium reactions, between 20 and 100 MeV out of equilibrium effects are important and above a 100 MeV direct reactions are dominant. The DYWAN model (DYnamical WAvelet in Nuclei) proposes a global description of these reactions and is able to account for the transition between the different processes. This model includes quantum effects, mean field dynamics and particle correlations (a complete description of the model can be found in [1]).

2.1.1 Dissipative behaviour

The global behaviour of the system is given by the one-body density matrix which evolution is given by the Extended Time Dependent Hartree Fock Equation :

$$i\dot{\rho} = [h(\rho), \rho] + iI(\rho), \tag{1}$$

where h is the one-body self consistent mean field, I is the collision term and ρ is the one body density matrix, $\rho = \sum_\lambda |\phi_\lambda >< \phi_\lambda|$, the $|\phi_\lambda >$ being the single-particle wavefunctions.

The initial state of the nucleus is prepared as follows: we start from a set of trial single particle (s.p.) wavefunctions which are expanded onto a wavelet basis :

$$|\phi_\lambda >= \sum_i \omega_i^\lambda |\alpha_i^\lambda >< \alpha_i^\lambda|. \tag{2}$$

An iterative procedure is then implemented, the one-body density matrix and the self consistent mean-field being constructed from the wavefunctions. To simulate the dynamics, the Eq. 1, is transcribed in terms of equations of motion for the non stationary wavelets: the mean field term corresponds to a set of coupled differential equations for the first and second moments in position and in momentum coordinates of the wavelets. The collision term corresponds to a master equation which rules the populations of single particle states, and therefore the weights of the wavelets. Due to this collision term the one body density matrix will become:

$$\rho = \sum_\lambda n_\lambda |\phi_\lambda >< \phi_\lambda| = \sum_i \sum_\lambda n_\lambda^i |\alpha_i^\lambda >< \alpha_i^\lambda|, \tag{3}$$

the n_λ^i varying between 0 and 1 during the dynamics. The orthogonality of the elements of the basis is conserved in time during the dynamics, which is essential to insure the Pauli-blocking.

2.1.2 Fluctuations

In order to describe fragment production, one must go beyond the one-body level. The complete description of a system of N fermions in interaction is given by the N body wavefunction. Within the mean-field approach, the N-body wavefunction can be written as a Slater determinant of s-p wavefunctions $|\Phi^N >= |\phi_{\lambda_1} > \wedge ... \wedge |\phi_{\lambda_a} >$ (the wedge product accounting for the antisymmetrization). Due to the orthonormality properties of wavelets, this Slater determinant can be written as a linear combination of Slater determinants of wavelets $|\Phi^N >= \sum_M |\theta_M >$, where $|\theta_M >= |\alpha_{i_1}^{\lambda_1} > \wedge ... \wedge |\alpha_{i_N}^{\lambda_N} >$ and M stands for a given set of indices $i_1, ..i_N$. When dissipative effects are included via the collision term in the ETDHF equation, the system is described by a statistical mixture of Slater determinants :

$$|\Psi^N >= \sum_K a_K(t) |\Phi_K^N >= \sum_K a_K(t) \sum_{M_K} |\theta_{M_K} > \tag{4}$$

with $|\theta_{M_K} >= |\alpha_{i_1}^{\lambda_{1K}} > \wedge .. \wedge |\alpha_{i_N}^{\lambda_{N_K}} >$. In order to be consistent with the maximum entropy condition the weights of the different Slater determinants of wavelets is chosen uniformely distributed. In this way Eq. 4 represents the least biased N-body wavefunction compatible with the one- and two-body information contained in Eq. 1. Each Slater determinant corresponds to a fluctuation around the mean behaviour, driven by the one-body density operator.

2.2 Mechanisms of reaction

2.2.1 Proton double differential cross section for $n + {}^{208}Pb$

The figure 1 shows the proton double differential cross section for the reaction $n + {}^{208}Pb$ at 96 MeV, at angles varying between 20 and 140 degrees. The crosses represent the experimental data and the full line the results of the simulation. In general, for most of models, double differential cross sections are particularly difficult to reproduce in the energy range between 20 and 100 MeV, since for these energies out of equilibrium effects are strong (as can be deduced from the important difference between the spectra at 20 and 140 degrees), while mean field effect cannot be neglected. The DYWAN simulation is in correct agreement with the experimental data for all angles. The discrepancy between theoretical and experimental data (deficit at low angles and excess at large angles) may be explained by the simplicity of the effective force used in the code. Indeed, at the present time, a simplified Skyrme interaction is implemented, this interaction being local and without surface terms. The use of a more refined effective force should have an appreciable impact on the results of the simulation, since the system is sensitive to any change in the physical parameters, as shown in the following sections.

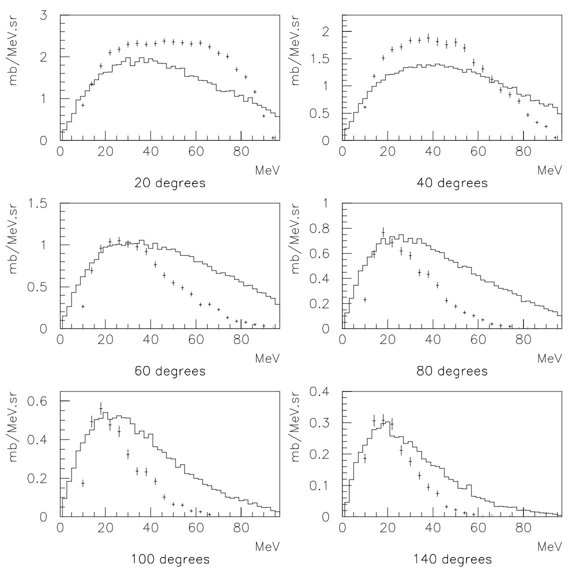

Figure 1: Proton double differential cross section for ${}^{208}Pb(n, xp)$ at 96 MeV. The full line corresponds to the simulated data and the crosses to the experimental data (LPC Caen, J.F. Lecolley, V. Blideanu).

2.2.2 Contribution of the different impact parameters

In the DYWAN model, the incident nucleon is described as a wave expanded onto a basis of wavelets. According to this decomposition, it is possible to select a range of impact parameters for the incoming nucleon. The figure 2 shows the proton double differential cross section for the n (96MeV) + ${}^{208}Pb$ for different ranges in impact parameter. These simulations show that peripheral collisions play an important role in the building of the spectra. Surface effects can therefore have a strong influence on these reactions.

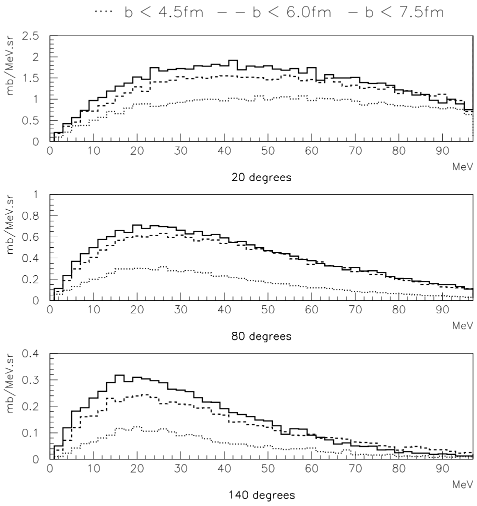

Figure 2: Proton double differential cross section for $^{208}Pb(n, xp)$ at 96 MeV for different ranges in impact parameter (full curve: $b < 7.5fm$, dashed curve: $b < 6fm$, dotted curve: $b < 4.5fm$).

2.2.3 Mean field effects

While many models implement a constant average potential well, in the DYWAN approach the mean field is computed self-consistently all along the dynamics. In order to see its influence, a simulation whith a constant mean field (the mean field of the initial nucleus) has been performed. The result is given in the figure 3. The left panel corresponds to the self-consistent calculation, as reference, and the central panel to the simulation with no self-consistency. For the lattest, the amplitude of the spectra is strongly decreased at small angles and roughly constant at large angles. This sensitivity can be explained by the importance of peripheral collisions: at the periphery the density of the target becomes of the same order of magnitude than the density of the incident nucleon, and therefore it is the region where the mean field of the initial nucleus will be the most affected by the incident wave. This result shows that mean field effects are not negligible especially for the emission at small angles.

2.2.4 Medium effects

In order to treat the collision term in Eq. 1, a free nucleon-nucleon cross section (angle and energy dependent) is used. Actually, this free nucleon-nucleon cross section should be modified by in-medium effects. It is still an open question to know how the in-medium effects affect the nucleon-nucleon cross section. We try the Machleidt and Li prescription whis is based upon a Dirac-Brueckner approach ([2]). It corresponds to a strong decrease of the nucleon-nucleon cross section (they are roughly divided by a factor 2). The right panel in figure 3 presents the result of a simulation using the Machleidt and Li cross section. The amplitude of the spectra is sensitive to the variation of the nucleon-nucleon cross section. There is a strong global decrease with regard to the reference (left panel) increasing the discrepancy between experimental and simulated data. A possible interpretation of this result is that the Machleidt prescription is rather too strong and that in-medium nucleon-nucleon cross section may not be very different from the free ones.

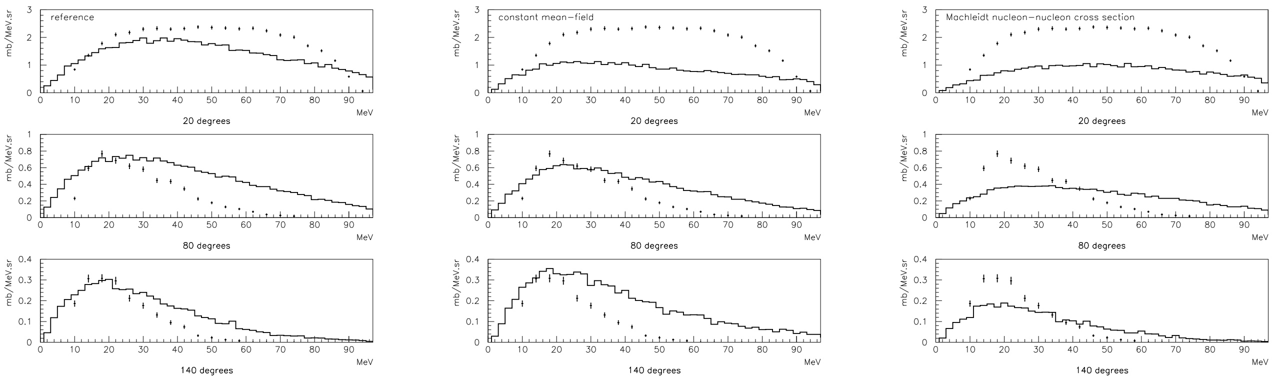

Figure 3: Proton double differential cross section for $^{208}Pb(n,xp)$ at 96 MeV for different prescriptions. The left panel is the reference, the central panel corresponds to a simulation without self-consistency, the right panel to a simulation with the Machleidt and Li nucleon-nucleon cross section ([2]) (full line: simulation, crosses: experimental data).

2.3 Cluster emission

In the DYWAN model, the nucleon and clusters emission are not treated independently, and therefore their production rate are linked. In principle, the formation of a cluster depends on its binding energy. Nonetheless, the calculations of the binding energy of all possible combinations of nucleons emitted by the remnant would be very time consuming. Therefore it is necessary to have a preliminary step able to make a fast pre-selection of the possible clusters. This pre-selection is performed thanks to a proximity criterium in phase space. The results of this preliminary step are presented in figure 4 which gives the double differential cross section for different clusters for the reaction p (63MeV)+ ^{208}Pb (experimental data from [3]). The order of magnitude and evolution of shape is correctly reproduced. The excess observed particularly at large angles should be reduced when a more refined procedure, computing binding energies, is utilised.

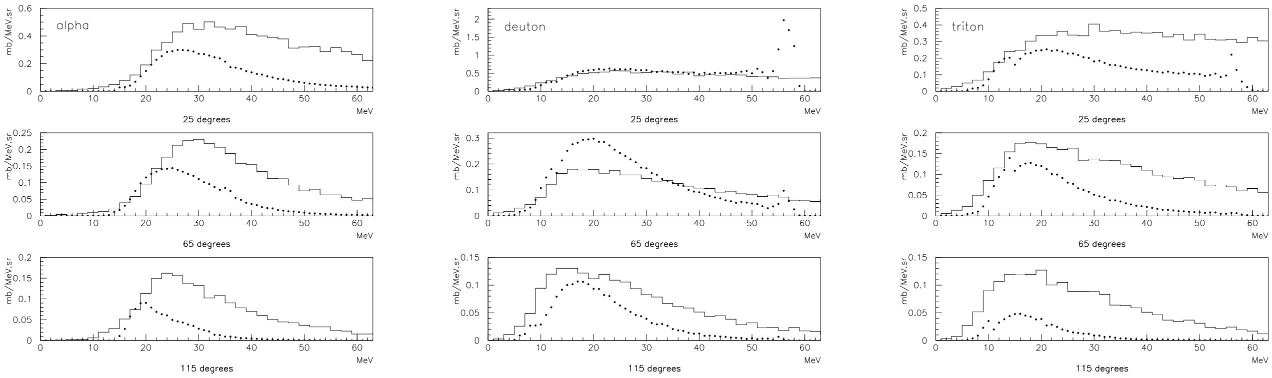

Figure 4: Double differential cross section for the reaction p(62.9MeV) + ^{208}Pb for different clusters, full line: simulation, dots: experimental data ([3]).

3 Description of light nucleus emission at low excitation energy with the Generalised Liquid drop Model

In this section, we will study the light nucleus emission as a tunneling process within a very asymmetric fission mode. The potential barriers are calculated from a Generalized Liquid Drop Model, using quasi-molecular shapes, previously developed to study the fusion ([4]) and fission processes ([5],[6]). Within this model, the separation in two fragments occurs rapidly for highly asymmetric fission, and therefore the one-body shapes play a minor role. The proximity forces in the neck between the fragments smooth strongly the unrealistic pure coulomb peak. The potential barrier top corresponds to two well separated spheres maintained in unstable equilibrium by the balance between the repulsive Coulomb forces and the attractive nuclear force (see figure 5). In this work, we will consider only excitation energy lower than the potential barrier height.

3.1 Partial half-lives for light nucleus emission

For the very asymmetric fission mode, the preformation probability at the surface is one. Consequently the decay constant for the light nucleus emission is simply:

$$\lambda = \nu_0 P. \tag{5}$$

The assault frequency ν_0 has been taken as

$$\nu_0 = 10^{20}\ s^{-1}. \tag{6}$$

The barrier penetrability P is calculated within the action integral

$$P = exp[-\frac{2}{\hbar}\int_{r_{in}}^{r_{out}} \sqrt{2B(r)(E(r)-E^*)dr}], \tag{7}$$

where r_{in} and r_{out} correspond to the points where $E(r) = E^*$ (see figure 5).

The inertia B(r) is related to the reduced mass by ([8]):

$$B(r) = \mu(1 + 1.3f(r)) \tag{8}$$

with

$$f(r) = \begin{cases} \sqrt{\frac{R_{cont}-r}{R_{cont}-R_{in}}}, r \leq R_{cont} \\ 0, r \geq R_{cont} \end{cases} \tag{9}$$

The partial half-life is finally obtained by

$$T_{1/2} = \frac{ln2}{\lambda}. \tag{10}$$

In preceding works [7, 8, 9] it has been shown that these procedures for determining the potential barriers and the partial half-lives allow to reproduce accurately the α and cluster emission half-lives. The rms deviation between the theoretical and experimental values of $log_{10}[T_{1/2}(s)]$ for 373 α emitters is only 0.63 and 0.35 for the subset of even-even nuclides (see Fig. 6).

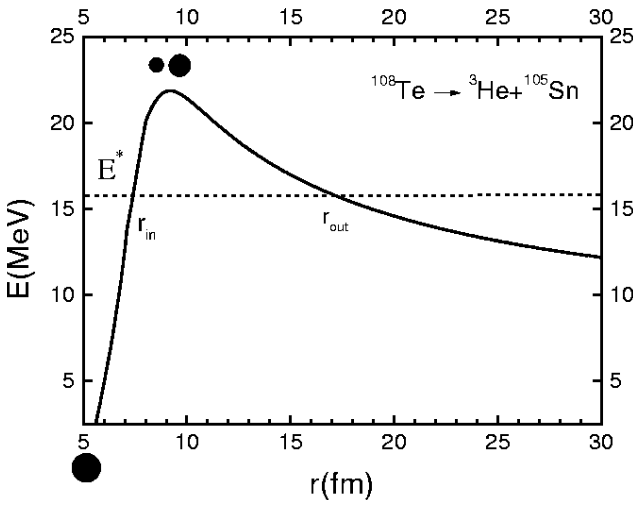

Figure 5: Potential barrier governing the ^3He emission from the ^{108}Te. E^* is the excitation energy and r_{in} and r_{out} the turning points. r is the center-of-mass distance.

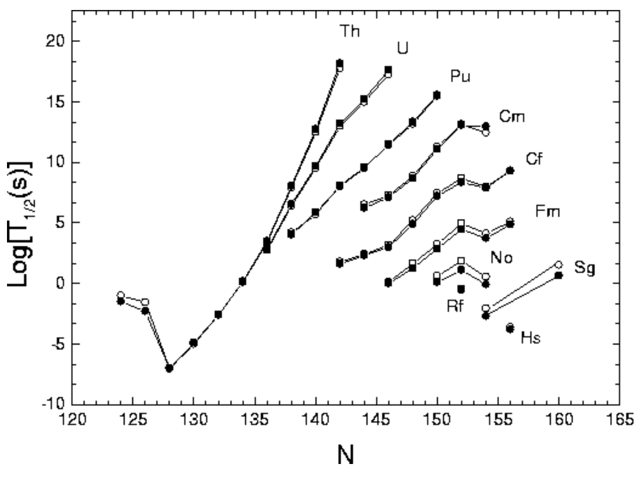

Figure 6: $log_{10}[T_{1/2}(s)]$ for the α emission from Th, U, Pu, Cm, Cf, Fm, No, Rf, Sg and Hs isotopes. The open and full circles correspond respectively to the experimental and theoretical data versus the neutron number N.

4 Analytical formulae for the α decay half-lives

The data set of 373 α emitters was used to establish, thanks to a fitting procedure, analytical formulae for the $log_{10}[T_{1/2}(s)]$ for α decay of non excited nucleus ([10]). The rms deviation between the results given by these formulae and experimental data is 0.285 for the even-Z even-N emitters, 0.39 for the odd-even, 0.36 for the odd-even and 0.35 for the odd-odd. These formulae have been extended so as to include excitation energy below the barrier. Due to the lack of experimental data, the fit was performed on $log_{10}[T_{1/2}(s)]$ obtained with the Generalized Liquid Drop Model. For the even Z- even N nuclei the following formula has been obtained with a rms deviation of 0.28 between the data set given by the GLDM and the values given by the formula:

$$log_{10}\left[T_{1/2}(s)\right] = (-25.31 - 1.1629A^{\frac{1}{6}}\sqrt{Z} + \frac{1.5864\,Z}{\sqrt{Q_\alpha + E^*}}) \times(1 - 4.5182\times 10^{-4}\,E^{*2}). \tag{11}$$

For the even-odd the following relation leads to a rms deviation of 0.41

$$log_{10}\left[T_{1/2}(s)\right] = (-26.65 - 1.0859A^{\frac{1}{6}}\sqrt{Z} + \frac{1.5848\,Z}{\sqrt{Q_\alpha + E^*}}) \times(1 + 1.1170\times 10^{-2}\,E^* - 1.4903\times 10^{-3}\,E^{*2}). \tag{12}$$

For the odd-even nuclei the rms deviation is 0.27

$$log_{10}\left[T_{1/2}(s)\right] = (-25.68 - 1.1423A^{\frac{1}{6}}\sqrt{Z} + \frac{1.592\,Z}{\sqrt{Q_\alpha + E^*}}) \times(1 + 8.9617\times 10^{-3}\,E^* - 1.3446\times 10^{-3}\,E^{*2}). \tag{13}$$

For the odd-odd nuclei the following formula leads to a rms deviation of 0.5

$$log_{10}\left[T_{1/2}(s)\right] = (-29.48 - 1.113A^{\frac{1}{6}}\sqrt{Z} + \frac{1.6971\,Z}{\sqrt{Q_\alpha + E^*}}) \times(1 - 8.8806\times 10^{-3}\,E^*). \tag{14}$$

The introduction of the excitation energy does not diminish the accuracy of the formulae.

5 Analytical formulae for the Be, Li, He, and H decay half-lives

For excitation energies below the potential barrier height the above-mentioned procedure has been applied for the Be, Li, He, and H decay half-lives ([10]).

For ${}^{9}_{4}Be$ the formula is, with a rms deviation of 0.48,

$$log_{10}\left[T_{1/2}(s)\right] = (-31.69 - 2.238A^{\frac{1}{6}}\sqrt{Z} + \frac{4.47183\,Z}{\sqrt{Q + E^*}}) \times(1 + 2.384\times 10^{-3}\,E^* - 9.556\times 10^{-5}\,E^{*2}). \tag{15}$$

For ${}^{7}_{3}Li$, with $\sigma = 0.38$,

$$log_{10}\left[T_{1/2}(s)\right] = (-27.55 - 1.796A^{\frac{1}{6}}\sqrt{Z} + \frac{3.0016\,Z}{\sqrt{Q+E^*}})$$
$$\times(1 + 2.665 \times 10^{-3}\,E^* - 1.109 \times 10^{-4}\,E^{*2}). \quad (16)$$

For ${}^{6}_{3}Li$, with $\sigma = 0.36$,

$$log_{10}\left[T_{1/2}(s)\right] = (-27.45 - 1.647A^{\frac{1}{6}}\sqrt{Z} + \frac{2.8051Z}{\sqrt{Q+E^*}})$$
$$\times(1 + 3.107 \times 10^{-3}\,E^* - 1.213 \times 10^{-4}\,E^{*2}). \quad (17)$$

For ${}^{6}_{2}He$, with $\sigma = 0.35$,

$$log_{10}\left[T_{1/2}(s)\right] = (-24.85 - 1.424A^{\frac{1}{6}}\sqrt{Z} + \frac{1.8773Z}{\sqrt{Q+E^*}})$$
$$\times(1 + 2.873 \times 10^{-3}\,E^* - 1.288 \times 10^{-4}\,E^{*2}). \quad (18)$$

For ${}^{3}_{2}He$, with $\sigma = 0.24$,

$$log_{10}\left[T_{1/2}(s)\right] = (-23.60 - 1.003A^{\frac{1}{6}}\sqrt{Z} + \frac{1.3665Z}{\sqrt{Q+E^*}})$$
$$\times(1 + 3.896 \times 10^{-3}\,E^* - 1.662 \times 10^{-4}\,E^{*2}). \quad (19)$$

For ${}^{3}_{1}H$, with $\sigma = 0.14$,

$$log_{10}\left[T_{1/2}(s)\right] = (-22.65 - 0.7187A^{\frac{1}{6}}\sqrt{Z} + \frac{0.6775Z}{\sqrt{Q+E^*}})$$
$$\times(1 + 3.079 \times 10^{-3}\,E^* - 1.795 \times 10^{-4}\,E^{*2}). \quad (20)$$

For ${}^{2}_{1}H$, with $\sigma = 0.16$,

$$log_{10}\left[T_{1/2}(s)\right] = (-22.02 - 0.6039A^{\frac{1}{6}}\sqrt{Z} + \frac{0.5626Z}{\sqrt{Q+E^*}})$$
$$\times(1 + 3.06 \times 10^{-3}\,E^* - 1.871 \times 10^{-4}\,E^{*2}). \quad (21)$$

For ${}^{1}_{1}H$, with $\sigma = 0.08$,

$$log_{10}\left[T_{1/2}(s)\right] = (-21.32 - 0.4214A^{\frac{1}{6}}\sqrt{Z} + \frac{0.3961Z}{\sqrt{Q+E^*}})$$
$$\times(1 + 1.208 \times 10^{-3}\,E^* - 9.972 \times 10^{-5}\,E^{*2}). \quad (22)$$

It is interesting to observe that the rms deviation remains low even for the highest asymmetries.

6 Conclusion

The DYWAN model can make qualitative and quantitative predictions on nucleon-nucleus collisions while giving us the possibility to investigate the mechanisms of the reaction. The model can be improved by introducing of a more refined effective force and by taking into account the binding energy in the cluster recognition. Even in the present state, the main features of the cluster emission are reproduced. The Generalized Liquid Drop Model can give the half-lives for a particular decay channel: emission of light nuclei below the barrier. The comparison with experimental data for the α particles shows the accuracy of these predictions. Analytical formulae based upon this approach are proposed, allowing to determine rapidly the partial-half life for the different clusters.

References

[1] Jouault B., Sébille F. and de la Mota V. 1998 *Nucl Phys.* A **628** 119.

[2] Li G. Q. and Machleidt R. 1993 *Phys. Rev.* C **48** 1702.

[3] Guertin A., *Ph.D. Thesis*, Université de Nantes (2001).

[4] Royer G. and Remaud B. 1985 *Nucl. Phys.* A **444** 477.

[5] Royer G. and Remaud B. 1984 *J. Phys.* G **10** 1057.

[6] Royer G. and Haddad F. 1995 *Phys. Rev* C **51** 2813.

[7] Royer G., Gupta R. K. and Denisov V. Y. 1998 *Nucl. Phys.* A **632** 275.

[8] Royer G. and Moustabchir R. 2001 *Nucl. Phys.* A **683** 182.

[9] Royer G. 2000 *J. Phys.* G **26** 1149.

[10] Bonilla C. and Royer G. 2003 *Heavy Ion Physics* **17/1** 49